Model for Determination of Protective Shielding Thickness for Diagnostic Radiology Rooms

P. R. Costa[1], L. V. E. Caldas[2]
[1] Instituto de Eletrotécnica e Energia /USP Av. Prof. Luciano Gualberto, 1289 - 05508-900 - São Paulo - Brazil.
pcosta@iee.usp.br
[2] Instituto de Pesquisas Energéticas e Nucleares/CNEN C.P. 11049 - 05422-970 - São Paulo - Brazil.
lcaldas@baitaca.ipen.br

INTRODUCTION

The NCRP 49 (1976) (1) standard presents a methodology to determine protective shielding for diagnostic and therapeutic X-ray rooms. This methodology has been reviewed by several authors in the recent years (2). This work presents contributions for this new shielding evaluation method, taking into account information regarding patient attenuation and scattering, as well as workload spectra for diagnostic imaging modalities. The main object of the investigation was the development of a method for determining the thickness of a given material required to correct attenuation of primary, scattered and leakage radiation spectra which reach a structural barrier in a radiological room. This methodology was combined to new information regarding spectral distributions of radiation scattered by a phantom in order to allow the determination of ambient dose equivalents in X-ray rooms. The product of this work consists of a model that provides an optimised treatment for the problem of determining shielding thickness of the barriers necessary for radiological room protection**.**

METHODOLOGY

Semi-empirical TBC model

Tucker *et. al.*(3) introduced a model (TBC model) which proposed two different formulations for the evaluation of the radiation spectra emitted by an X-ray tube. These formulations take into account the continuous (*Bremsstrahlung*) spectra and the characteristic emission. The TBC model considered the target material, the tube design, and the composition of the materials which attenuate the radiation beam before emerging from the tube housing. The equation adopted for the *Bremsstrahlung* contribution was:

$$N^B(E)dE = \frac{\sigma_0 Z^2}{A}\frac{dE}{E}\int_E^{T_0}\frac{B(E,T)}{T}F(E,T)\left(\frac{1}{\rho}\frac{dT}{dx}\right)^{-1}dT \qquad (1)$$

Where $\sigma_0 = \alpha r_e^2$, with α as the fine structure constant and r_e the classical radius of the electron. Moreover, Z is the effective atomic number of the target material, A is the atomic mass of the target atoms, T_0 is the kinetic energy of the electrons when they reach the target, T is the kinetic energy of the electrons inside the target at a distance x of the surface, and E is the energy of the photons produced by the electrons. The expression $(1/\rho)(dT/dx)$ represents the mass stopping power of the target material, B(E,T) is a function proportional to the number of photons produced by each incident electron, and F(E,T) represents the filtration of the materials.

The TBC model proposed the function J(x/R) to represent the probability for characteristic emission. This probability was modelled as a parabolic function which drops to zero when the electron energy is equal to the k-edge bind energy, E_K, or

$$J(x/R) = \begin{cases}\left(\frac{3}{2}\right)\left[1-\left(\frac{x}{R}\right)^2\right] & \text{for } x \le R \\ 0 & \text{for } x > R\end{cases} \qquad (2)$$

R is the distance inside the target where the electron average kinetic energy is equal to E_k. Therefore, the characteristic radiation production can be modelled as

$$N^c(E_i) = A_k\left(\frac{T_0}{E_k}-1\right)^{n_k} f(E_i)\int_0^R J\left(\frac{x}{R}\right)\cdot e^{-\mu_W(E_i)x/\operatorname{sen}\theta}dx \qquad (3)$$

A_k and n_k are model parameters obtained by using a non-linear least square method, and $f(E_i)$ is the fractional X-ray characteristic emission of photons with energy E_i. The parameter A_k represents the number of characteristic photons emitted by the incident electrons. Moreover, the distance R can be calculated as $R=(T_0^2-E_k^2)/\rho C(T_0)$ where C(T) is the Thomson-Whiddington constant. In the present work, the Birch and Marshall (4) data for this constant were fitted by a linear function using the least square method.

Waveform generalised model

The TBC waveform generalised model can be determined taking into account the applied voltage waveform represented by the following equation

$$V(t) = \frac{1}{f}\sum_{j=1}^{f} V_{max}\left|\text{sen}\left[\pi\left(12.10^{-3}\,t - \frac{j-1}{f}\right)\right]\right| \qquad (4)$$

In this equation, V_{max} is the peak potential in kVp units, t is the time interval during the exposure in milliseconds, and f is a parameter representative of the frequency of the high voltage generator.

The equations (1) to (4) provide the basis for the waveform-generalised model. This approach considers the high voltage applied to the tube as a function of the exposure time and calculates a series of elemental TBC spectra for each time interval. This formulation can be resumed by the equation

$$N_p^{\phi}(E) = \sum_{t=0}^{t_{exp}} N(E, V(t)) \qquad (5)$$

where t_{exp} is the time exposure selected in the X-ray machine.

Calibration in SI units

The X-ray spectra must to be calibrated using dosimetric units that can be related to functional parameters of the X-ray machine in order to be useful to the purpose of the present work. To perform this calibration, the definition of the quantity air kerma (5) normalised by the tube workload (mGy/mA.min) can be used and is given by

$$D^{\phi}(V) = C^{\phi}(V)\int_0^V N_p^{\phi}(E)\left(\frac{\mu(E)}{\rho}\right)_{air} E_{tr}^{m}(E)dE \qquad (6)$$

In this equation, the function $C^{\phi}(V)$ provides the normalisation of the radiation spectra in units of mGy/mA.min. Moreover, $(\mu(E)/\rho)_{air}$ represents the mass attenuation coefficient for air, and E^{m}_{tr} is the mean energy transferred to electrons of the medium. The function $C^{\phi}(V)$ can be calculated as:

$$C^{\phi}(V) = \frac{A^{\phi}\cdot V^{B^{\phi}}}{\int_0^V N_p^{\phi}(E)\left(\frac{\mu(E)}{\rho}\right)_{ar} E_{tr}^{m}(E)dE} \qquad (7)$$

Using equations (5) and (7), the calibrated X-ray spectra can be evaluated by

$$N_{p,n}^{\phi,V}(E) = C^{\phi}(V)\cdot N_p^{\phi}(E) \qquad (8)$$

Experimental verification

The experimental verification of the spectra provided by the application of the equations (1) and (3) was performed by comparison of computer simulations of this formulation with experimental measurements performed by using a PIN photodiode operating at room temperature. The experimental methodology and instrumentation was presented by Terini *et. al.*(6). The energy resolution of the photodiode measurements was about 3 keV. Experimental measurements performed by Fewell (7) at the Center for Devices and Radiological Health/US-Food and Drug Administration laboratories were also used. The radiation spectra measured by Fewell using a Ge(Li) detector were standardised considering the IEC 1267 (8) and NIST (9) high voltage and HVL set-up conditions. Table 1 shows the experimental conditions used for the comparison. Figures 1 and 2 present comparisons of TBC waveform generalised model and experimental results from Terini *et. al.*(6). Figures 3 and 4 show comparisons using data obtained by Fewell (7) and Table 2 presents the used experimental conditions.

Table 1 – Experimental conditions used during measurements of spectra showed in Figures 1 and 2. The X-ray equipment was composed by a Siemens Heliophos 4B HV transformer coupled to a 150/30/50 Rörix X-ray tube. The system was operated in fluoroscopic mode in these measurements. The computer simulated spectra used the same parameters to evaluate the generalised semi-empirical spectra showed as continuos lines in the figures.

VOLTAGE [kVp]	CURRENT (mA)	ADDITIONAL FILTRATION		RIPPLE (%)
		mm Al	mm Cu	
60	~ 2	3.4	0.6	~2
73	~ 2	1.2	0	~2

Table 2 – Experimental conditions used by Fewell (7) to obtain the radiation spectra presented in Figures 3 and 4. The corresponding TBC generated spectra used the same voltage parameters and inherent and added filtration choice in order to determine equivalent first and second half-value layers.

BEAM	VOLTAGE (kVp)	HVL BY FEWELL (mm Al)		HVL BY COMPUTER SIMULATION (mm Al)		TOTAL FILTRATION USED BY FEWELL (mm Al)	TOTAL FILTRATION ADOPTED FOR CALCULATION (mm Al)
		1st HVL	2nd HVL	1st HVL	2nd HVL		
IEC80	80	2.59	6.52	2.59	6.42	2.48	2.84
M100	100	4.89	11.61	4.89	11.42	5.258	6.25

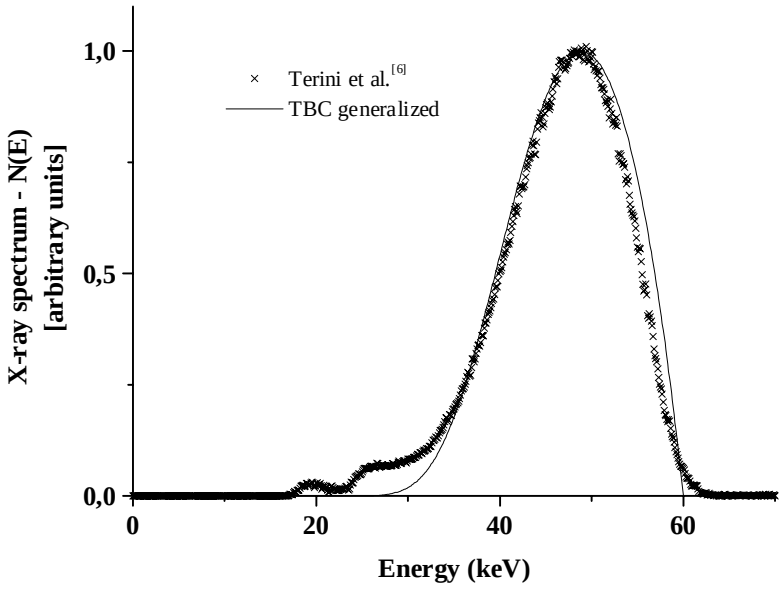

Figure 1 – Comparative results between measurements performed by a Si photodiode operated at room temprature (6) and computer simulation using the waveform generalised TBC model. The experimental conditions are presented in Table 1 for of 60 kVp, and they were the same used for the computer simulation.

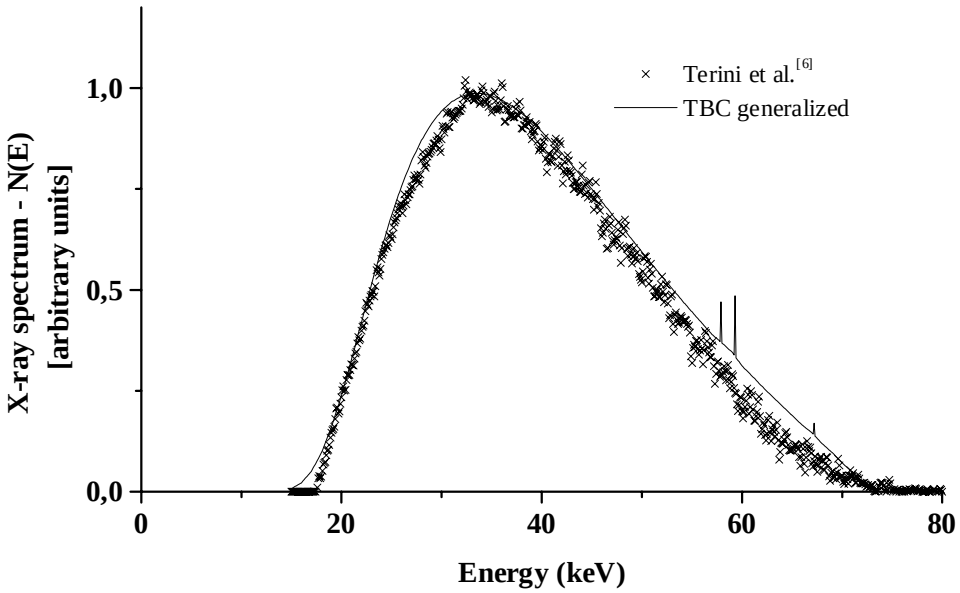

Figure 2 – Comparative results between measurements performed by a Si photodiode operated at room temprature (6) and computer simulation using the waveform generalised TBC model. The experimental conditions are presented in Table 1 for 73 kVp, and they were the same used for the computer simulation.

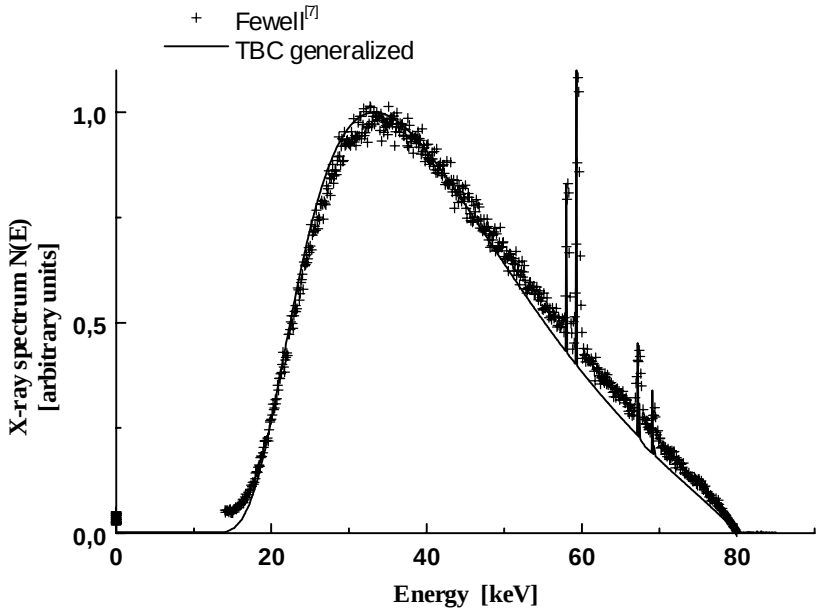

Figure 3 - Comparative results between Ge detector measurements (7) and computer simulation using the waveform generalised TBC model. The experimental conditions are presented in Table 2 for 80kVp, and they were the same used for the computer simulation.

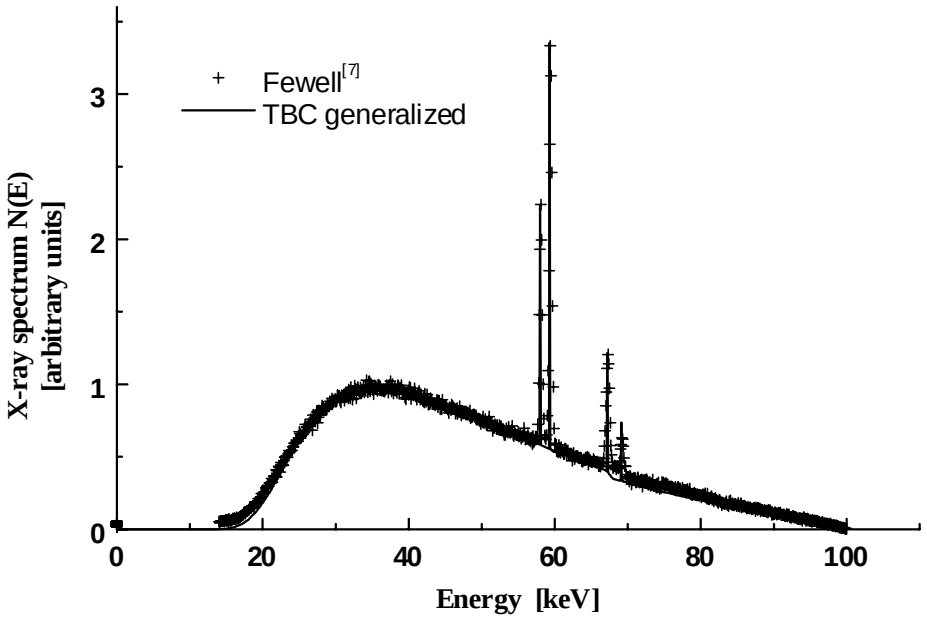

Figure 4 - Comparative results between Ge detector measurements (7) and computer simulation using the waveform generalised TBC model. The experimental conditions are presented in Table 2 for high voltage of 100 kVp, and they were the same used for the computer simulation.

Optimised model for shielding barriers calculation

The current radiation protection standards (10) propose the use of the quantity equivalent ambient dose in order to quantify the efficiency of a given radiation shielding. The present work introduces the following function to represent the primary radiation levels in terms of equivalent ambient dose at a distance of one meter of the focal spot:

$$H_p^{m,\phi}(10,x_p)=\sum_V\int_0^V\left(\frac{H^*(10)}{K_{ar}}\right)(E)N_{p,n}^{\phi,V}(E)W(V)e^{-\mu_m(E)x_p}dE=H_p^{0,\phi}(10)\left[\left(1+\frac{\beta_p^m}{\alpha_p^m}\right)e^{\alpha_p^m\gamma_p^m x_p}-\frac{\beta_p^m}{\alpha_p^m}\right]^{-\frac{1}{\gamma_p^m}} \quad (9)$$

where

$$H_p^{0,\phi}(10)=\sum_V\int_0^V\left(\frac{H^*(10)}{K_{ar}}\right)(E)N_{p,n}^{\phi,V}(E)W(V)dE \quad (10)$$

In the same way, expressions can be defined for scattered radiation as:

$$H_{e,\theta}^{m,\phi}(10,x_e)=\sum_V a'(V,\theta)\times10^{-6}\frac{F}{d_F^2}\int_0^V\left(\frac{H^*(10)}{K_{ar}}\right)(E)N_e^{\phi,V}(E,\theta)W(V)e^{-\mu^m(E)x_e}dE \quad (11)$$

where

$$a'(V,\theta)=\frac{10^6}{F'}\frac{\int_0^{E_{max}}\left(\frac{H^*(10)}{K_{ar}}\right)(E)N_e^{\phi,V}(E,\theta)W(V)dE}{\int_0^{E_{max}}\left(\frac{H^*(10)}{K_{ar}}\right)(E)N_p^{\phi,V}(E)W(V)dE} \quad (12)$$

and for leakage radiation as:

$$H_f^{m,\phi}(10, x_f) = L\left(\frac{H^*(d10}{K_{ar}}\right)_{V_{max}}^{x_{Pb}} \frac{\sum_V \int_0^V \left(\frac{H^*(10)}{K_{ar}}\right)(E) N_{p,n}^{\phi,V}(E) W(V) e^{-\mu_{Pb}(E)x_c} e^{-\mu_m(E)x_f} dE}{I_{max} \cdot 60 \int_0^{V_{max}} \left(\frac{H^*(10)}{K_{ar}}\right)(E) N_{p,n}^{\phi,V_{max}}(E) e^{-\mu_{Pb}(E)x_c} dE} \quad (13)$$

In these equations, $(H^*(10)/K_{ar})(E)$ provides the unity conversion from air kerma units (gray) to equivalent ambient dose (sievert) (11). The constants α^m_p, β^m_p and γ^m_p are obtained by applying Archer's model (2) for the utilised shielding material. The use of this model is especially useful in cases where the linear attenuation coefficient of the shielding material, $\mu_m(E)$, is not known. In this case, a non-linear least square method is applied two times: first, in order to fit families of attenuation curves of the considered material; second, in order to obtain workload related curves (equations (9) to (13)) calibrated in equivalent ambient dose units, which can be directly used for the shielding purpose. The function W(V) represents the workload spectrum (12) for the considered diagnostic modality and charge of use for the X-ray equipment. This formulation was chosen because of its ability to compensate the variation of the spectral shape when the radiation beam crosses the shielded wall .

Therefore, a generic shielding barrier can be obtained using the following inequality:

$$\frac{H_p^{m,\phi}(10, x_t^m)}{d_p^2} \cdot U + \left[\frac{H_{e,\theta}^{m,\phi}(10, x_t^m)}{d_e^2} + \frac{H_f^{m,\phi}(10, x_t^m)}{d_f^2}\right] \cdot (1 - U) \leq \frac{P}{T} \quad (14)$$

Solving this inequation to x_t, the shielding thickness can be determined, providing the optimised radiation level in the room's neighbourhood for a given workload spectrum.

RESULTS

A screening of workload spectra were realized in 14 Brazilian imaging departments using two different methods for data collection, which included General Radiography, Chest Radiography, Cardiac Angiography, Mammography and Computed Tomography dedicated radiation rooms. The Method I uses data collected by observing the operational techniques used in 605 examinations. The data corresponding to Method II were obtained by interviewing 51 technicians, who were questioned about the most useful parameters selected for the considered examinations.

The results were compared to Simpkin[12] data (Figure 5) and used to obtain attenuation curves for primary and secondary shielding calculations. Figure 6 shows attenuation curves for primary beams from General Radiography, Chest and Cardiac Angiography techniques. Similar curves can be obtained for secondary radiation (Figure 7).

Families of attenuation curves were also obtained for a commercial shielding material (not lead). These curves (Figure 8) were obtained by applying Archer's model to attenuation measurements. The Archer's model parameters were obtained by a non-linear least square method and used in the equations (9) to (13). The application of Archer's model provided a collection of workload spectra related curves for a commercial shielding material (Figure 9)[13].

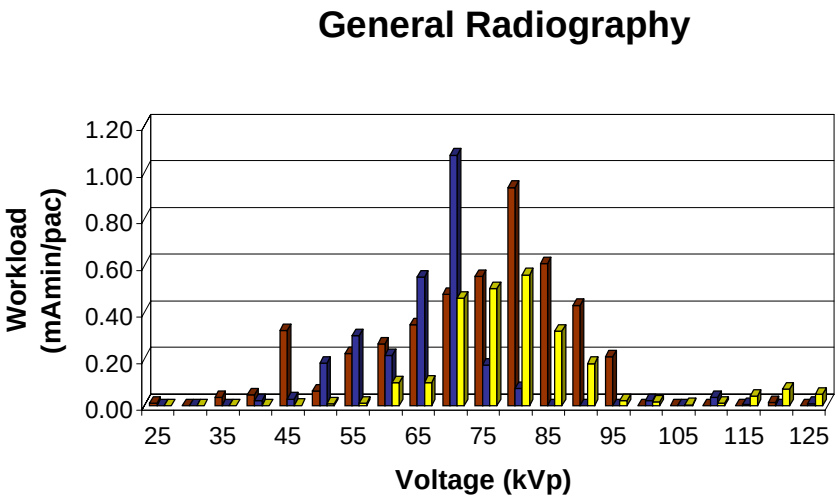

Figure 5 – Workload spectra obtained for the present work by Method I (red), Method II (blue) and published by Simpkin (12) for General Radiography technique.

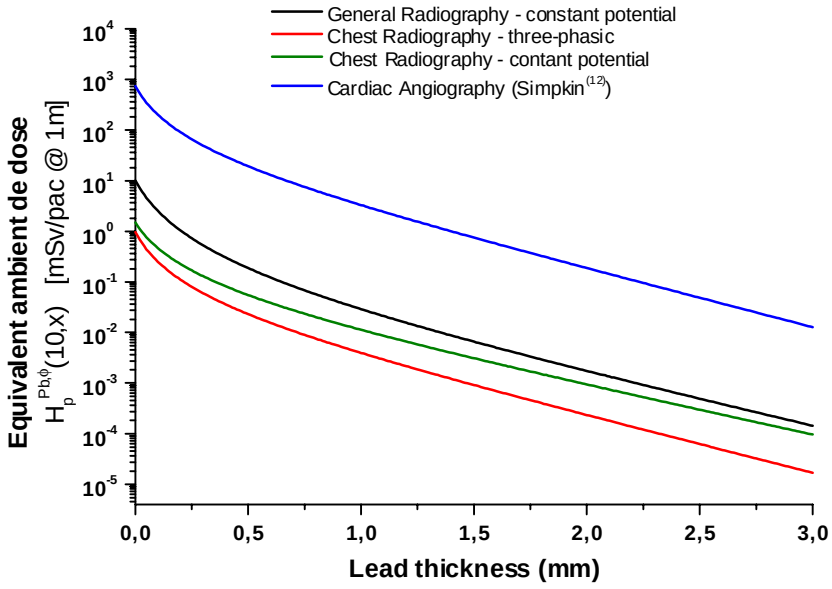

Figure 6 – Equivalent ambient dose as a function of lead thickness for primary radiation obtained applying equation (9) using workload spectra for General Radiography, Chest and Cardiac Angiography techniques.

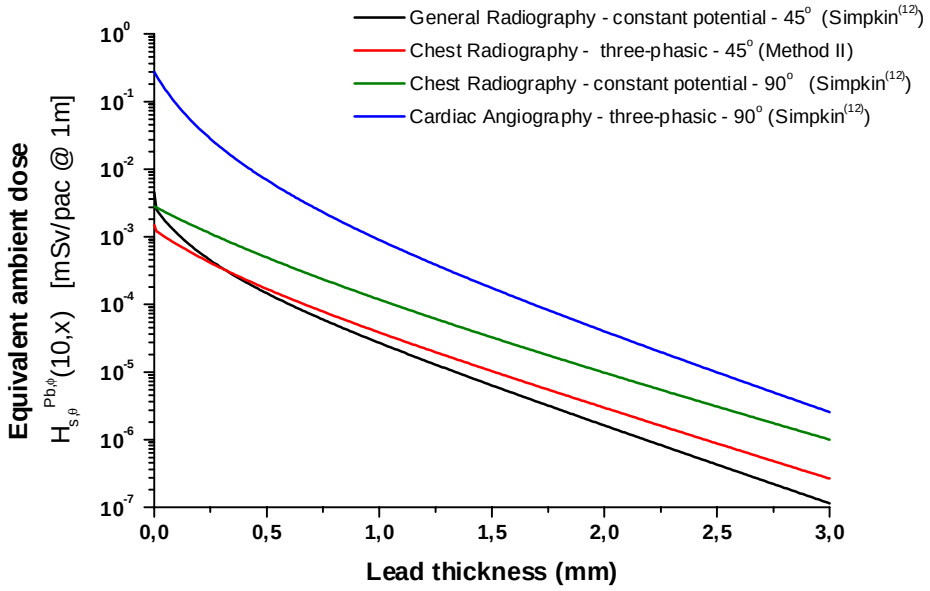

Figure 7 - Equivalent ambient dose as a function of lead thickness for secondary radiation obtained applying equations (11) to (13) using workload spectra for General and Chest Radiography considering a scattering angle of 45º and Cardiac Angiography technique considering a scattering angle of 90º. The considered workload spectra were obtained from Method II and from Simpkin (12).

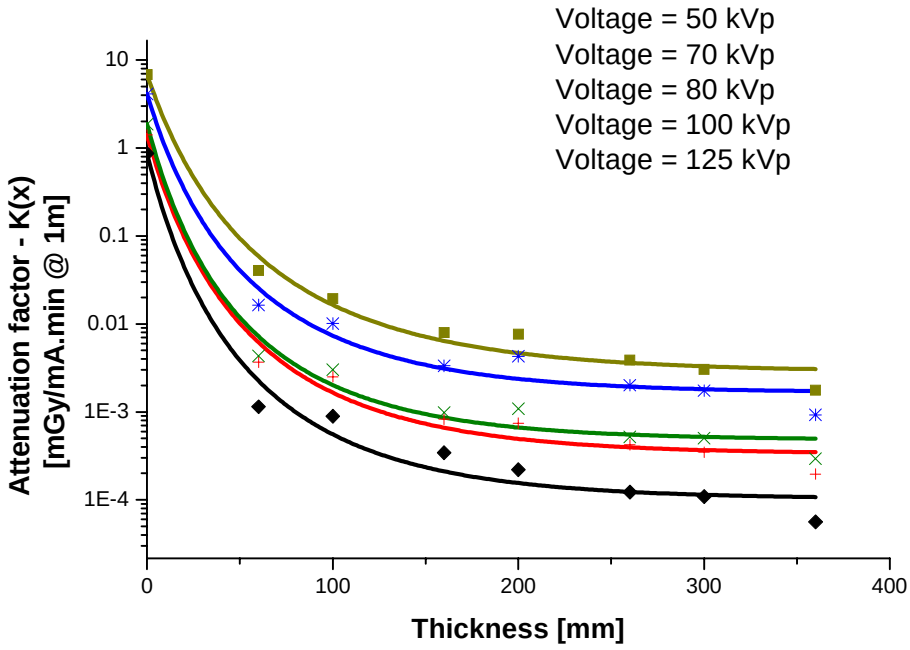

Figure 8 – Measured (points) and fitted (continuous lines) attenuation curves of a commercial shielding material. The fits were obtained applying Archer's model to experimentally measured data using a non-linear least square method

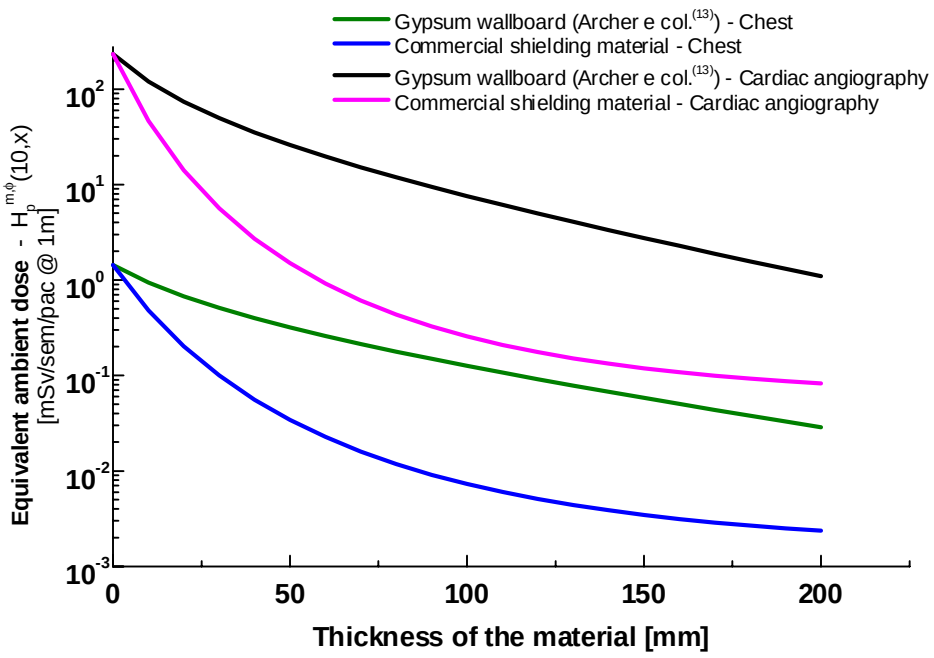

Figure 9 – Equivalent ambient dose for primary radiation using commercial shielding materials (not lead) and workload spectra for Chest and Cardiac Angiography techniques. These workloads were obtained from Simpkin(12). The Archer's model coefficients, α, β and γ, for the evaluated material were obtained applying the non-linear least square method in the data shown in Figure 8. The coefficients for the gypsum wallboard are from reference (13).

CONCLUSIONS

The work provides an optimised treatment for the problem of determining shielding barriers necessary for radiological room protection. The developed method associates information regarding primary and scattered spectra usually present during diagnostic procedures as well as new data from workload spectra. These information were resumed in a set of equations which provides the relationship between equivalent ambient dose and thickness of a shielding material considering primary, scattered and leakage radiations from a given diagnostic procedure. The equations can generate families of attenuation curves, which are very useful during diagnostic room shielding designs.

Comparative results of application of the NCRP 49 method and the formulation presented in this work in two real imaging diagnostic departments show a cost reduction of around 50% when using the optimised process. This result demonstrates that the development of an optimised methodology for shielding calculation in diagnostic room can be associated to a cost-benefit analysis.

ACKNOWLEDGMENTS

The authors gratefully acknowledge the contributions of Dr. Sílvio B. Herdade, Dr. Ricardo A. Terini and Mrs. Márcia C. Silva during several parts of this work. Thanks are also due to Mrs. Denise Y. Nersissian and Mr. Marco A. G. Pereira for the helpful discussions and suggestions during the development of the generalised model. Our very special thanks are to Dr. Thomas Fewell, from CDRH/FDA, who kindly provided some of the spectral data used in this work.

This work was supported by Fundação de Amparo à Pesquisa do Estado de São Paulo and Conselho Nacional de Desenvolvimento Científico e Tecnológico, Brasil.

REFERENCES

[1] NATIONAL COUNCIL ON RADIATION PROTECTION AND MEASUREMENTS. ***Structural Shielding Design and Evaluation for Medical Use of X rays and Gamma Rays of Energies up to 10 MeV***. NCRP Publications, Bethesda, MD, 1976 (NCRP Report 49).

[2] ARCHER, B.R. Diagnostic X-ray Shielding Design – New Data and Concepts. *in* D. FREY and P. SPRAWS, eds. ***The Expanding Role in Medical Physics in Diagnostic Imaging***. Proceedings of the 1997 AAPM Summer School. Advanced Medical Publishing, Wisconsin, Madison, 1997.

[3] TUCKER, D. M.; BARNES, G.T.; CHAKRABORTY, D.P. Semiempirical Model for Generating Tungsten Target X-ray Spectra. ***Medical Physics***, v.18, n.2, p.211-218, 1991.

[4] BIRCH, R..; MARSHALL, M. Computation of Bremsstrahlung X-ray Spectra and Comparison with Spectra Measured with a Ge(Li) Detector. ***Physics in Medicine and Biology***, v. 24, n. 3, p. 505-517, 1979.

[5] JOHNS, H. E.; CUNNINGHAN, J. R. "The Physics of Radiology," 4th ed., Charles C. Thomas Publ., Springfield (1983).

[6] TERINI, R.A.; COSTA, P.R.; FURQUIM, T.A.C.; HERDADE, S.B. Measurements of Discrete and Continuous X-ray Spectra with a Photodiode at Room Temperature. ***Applied Radiation and Isotopes***, v. 50, p. 343-353, 1999

[7] FEWELL, T.R. Personal communication, 1998.

[8] INTERNATIONAL ELECTROTECHNICAL COMMISSION. "Medical Diagnostic X-ray Equipment – Radiation Condition for Use in the Determination of Characteristics". Genève (1994) (IEC1267).

[9] CRICKENBERGER, J.M. Calibration Laboratories Technical Guide. NIST-National Institute for Science and Technology, U. S. Department of Commerce, USA (1995).

[10] INTERNATIONAL COMMISSION ON RADIOLOGICAL UNITS AND MEASUREMENTS. ***Conversion Coefficients for use in Radiological Protection Against External Radiation.*** Bethesda, MD, 1998. (ICRU Report 57)

[11] INTERNATIONAL COMMISSION ON RADIOLOGICAL UNITS AND MEASUREMENTS. ***Measurement of Dose Equivalents from External Photon and Electron Radiations***. Bethesda, MD, 1992. (ICRU Report 47).

[12] SIMPKIN, D. Evaluation of NCRP Report No. 49 Assumptions on Workloads and Use Factors in Diagnostic Radiology Facilities. ***Medical Physics***, v. 23, n.4, p.577-584, 1996.

[13] ARCHER, B.R.; FEWELL, T.R.; CONWAY,B.J.; QUINN,P.W. Attenuation Properties of Diagnostic X-ray Shielding Materials. ***Medical Physics***, v. 21, n.9, p.1499-1507, 1994.